

Role of fragment orientations in the formation of fusion valleys of superheavy elements

Ş. Mişicu and W. Greiner

Institut für Theoretische Physik, J.W.v.-Goethe Universität, Robert-Mayer Strasse 8-10, D-60325 Frankfurt am Main, Germany

(Received 14 June 2002; published 9 October 2002)

The dependence of the heavy-ion interaction on the orientation is investigated for the cold fusion of two (spherical or deformed) nuclei leading to a superheavy element. In contrast to the case of cold fission, when the fragments are exclusively emerging at scission in pole-pole configuration, in the case of cold fusion the fragments are not necessarily limited to a particular reciprocal orientation and capture can occur also for configurations other than the pole-pole configuration. The occurrence of minima in the driving potential as a function of the interfragment distance and of the mass asymmetry is discussed for several orientations.

DOI: 10.1103/PhysRevC.66.044606

PACS number(s): 25.70.Jj, 27.90.+b

I. INTRODUCTION

The cold fission configuration after the preformation of the fragments and rupture of the neck and the cold fusion configuration after the capture took place and before the mass transfer between the colliding emergent nuclei is initiated have similar features. In both cases, one speaks about a long- or short-lived dinuclear or quasimolecular system [1].

It was advocated long time ago that in the collision between a deformed target and a spherical projectile, the most favorable orientation of the deformed nucleus is the one in which its symmetry axis intersects the center of the spherical partner because it leads to a substantially lower fusion barrier than expected for a spherical nucleus of equal mass [2]. Thus, fusion becomes possible at lower bombarding energies, the probability for producing *cold* compound nuclei being enhanced. As for the binary cold fission, the lowest barrier corresponds to the alignment of the symmetry axes of both emerging fragments (see Fig. 4 of Ref. [3]). Using this mutual orientation of the fragments it was possible to describe the gross features of the mass-yield distribution in binary cold fission [4]. More recently it was invoked that fusion of two well-deformed nuclei in an equatorial-equatorial and equator-equator twisted orientation could be envisioned because such a configuration would be more compact than all other orientations of the two deformed nuclei [5].

The effect of orientation in nuclear reactions at low energy was also studied for symmetric quasimolecular systems such as $^{24}\text{Mg} + ^{24}\text{Mg}$ [6,7]. In this case stable configurations were found in pole-pole orientations. For the dinuclear molecule $^{12}\text{C} + ^{12}\text{C}$, due to the large oblate deformation of ^{12}C an equator-equator configuration explained the intermediate resonances seen in the experiment [8].

There is no doubt that the way in which the superheavy elements are synthesized is dependent also on particular deformations and orientations, as already noted in Ref. [5]. In analogy to the cold fission of ^{252}Cf we investigate the role of the fragments deformations and orientations on the driving potential of some superheavy elements such as $^{286}112$, $^{292}114$, $^{296}116$, and $^{306}122$.

II. ORIENTATION DEPENDENCE OF THE HEAVY-ION POTENTIAL

In previous works on cold fission, we computed the interaction potential between two heavy ions with densities ρ_1 and ρ_2 and center of masses separated by the distance \mathbf{R} , via a double-folding integral (see Ref. [9], and references therein),

$$V(\mathbf{R}) = \int d\mathbf{r}_1 \int d\mathbf{r}_2 \rho_1(\mathbf{r}_1) \rho_2(\mathbf{r}_2) v(s), \quad (1)$$

where $s = \mathbf{R} + \mathbf{r}_2 - \mathbf{r}_1$. The evaluation of the above folding integral is facilitated by the convolution theorem that states that the Fourier transform of the folded quantity is simply the product of the transforms of the individual component functions [10]. Defining the Fourier transform of a function $f(\mathbf{r})$ by

$$\tilde{f}(\mathbf{q}) = \int d\mathbf{r} \exp(i\mathbf{q} \cdot \mathbf{r}) f(\mathbf{r}), \quad (2)$$

the double-folding integral (1) becomes

$$V(\mathbf{R}) = (2\pi)^{-3} \int d\mathbf{q} \tilde{V}(\mathbf{q}) \exp(-i\mathbf{q} \cdot \mathbf{R}), \quad (3)$$

where the Fourier transform of the double-folding potential reads

$$\tilde{V}(\mathbf{q}) = \tilde{\rho}_1(\mathbf{q}) \tilde{\rho}_2(-\mathbf{q}) \tilde{v}(\mathbf{q}). \quad (4)$$

Consider the geometry from Fig. 1, where the primed axis corresponds to the molecular (dinuclear system) frame and the double primed to the body-fixed framed of each nucleus. The density distribution $\rho_i(\mathbf{r}')$ ($i=1,2$) in the molecular frame is related to that in the body-fixed frame by Euler rotations,

$$\rho_i(\mathbf{r}') = \mathcal{R}(\alpha_i, \beta_i, \gamma_i) \rho_i(\mathbf{r}''). \quad (5)$$

We assume that the density distribution in the body-fixed frame, $\rho_i(\mathbf{r}'')$, is axially symmetric,

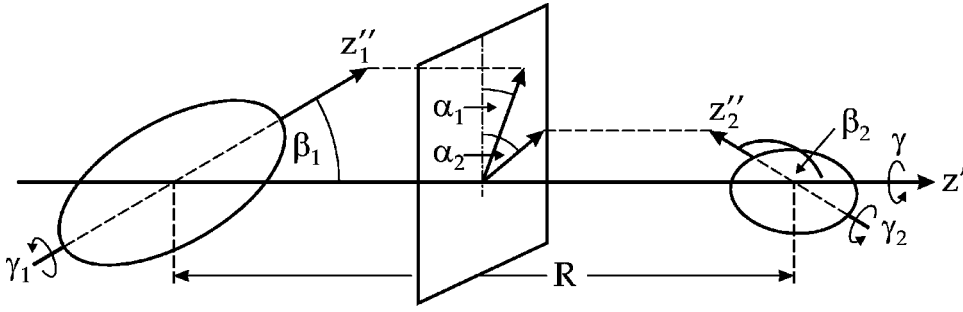


FIG. 1. The position and space orientation of two colliding nuclei are described by the center-to-center distance and the Euler angles $\alpha_i, \beta_i, \gamma_i$. The axis z' is the third axis of the molecular frame. The double-primed axes correspond to the intrinsic frame of each nucleus.

$$\rho_i(\mathbf{r}'') = \sum_{\lambda} \rho_{\lambda}(r''_i) Y_{\lambda 0}(\hat{r}''_i), \quad (6)$$

and that its shape is given by a Fermi distribution

$$\rho_i(\mathbf{r}'') = \frac{\rho_0}{1 + e^{(r''_i - c_i)/a}}, \quad (7)$$

with $c_i = c_0 [1 + \sum_{\lambda \geq 2} \beta_{\lambda} Y_{\lambda 0}(\hat{r}''_i)]$. The constant ρ_0 is fixed by normalizing the proton and neutron density to the Z_i proton and N_i neutron numbers, respectively. This condition ensures the volume conservation. The half radius c_0 and the diffusivity a are taken from the liquid drop model [11].

The spherical harmonics behave under Euler rotations [12], according to

$$\mathcal{R}(\alpha_i, \beta_i, \gamma_i) Y_{lm'}(\theta, \phi) = \sum_m Y_{lm}(\theta, \phi) D_{mm'}^l(\alpha_i, \beta_i, \gamma_i). \quad (8)$$

Thus

$$\rho(\mathbf{r}'_i) = \sum_{\lambda \mu} \rho_{\lambda}(r_i) D_{\mu 0}^{\lambda}(\alpha_i, \beta_i, \gamma_i) Y_{\lambda \mu}(\hat{r}'_i). \quad (9)$$

The Fourier transform of the density distribution $\tilde{\rho}(\mathbf{q}) = \int d\mathbf{r} \rho(\mathbf{r}) \exp(i\mathbf{q} \cdot \mathbf{r})$, occurring in Eq. (4), can be calculated using the plane wave expansion

$$\exp(i\mathbf{q} \cdot \mathbf{r}) = 4\pi \sum_{lm} i^l j_l(qr) Y_{lm}^*(\Omega_q) Y_{lm}(\hat{r}), \quad (10)$$

which leads to the final expression

$$\tilde{\rho}(\pm \mathbf{q}) = 4\pi \sum_{\lambda \mu} (\pm i)^{\lambda} D_{\mu 0}^{\lambda}(\alpha_i, \beta_i, \gamma_i) Y_{\lambda \mu}(\Omega_q) \tilde{\rho}_{\lambda}(q), \quad (11)$$

where

$$\tilde{\rho}_{\lambda}(q) = 4\pi \int dr r^2 \rho_{\lambda}(r) j_{\lambda}(qr). \quad (12)$$

The Fourier transform of the nucleon-nucleon interaction reads

$$\tilde{v}(\mathbf{q}) = \int ds v(s) \exp(i\mathbf{q} \cdot \mathbf{s}) = 4\pi \int dr s^2 j_0(qs) v(s). \quad (13)$$

The Fourier transform of the double-folding potential is obtained by inserting Eqs. (13) and (11) in Eq. (4),

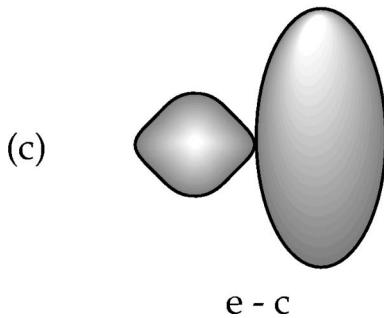
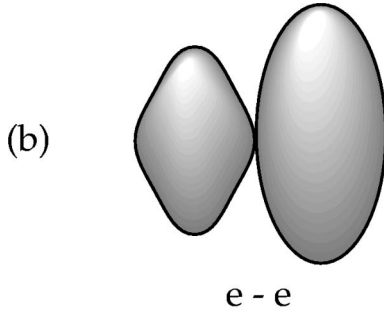
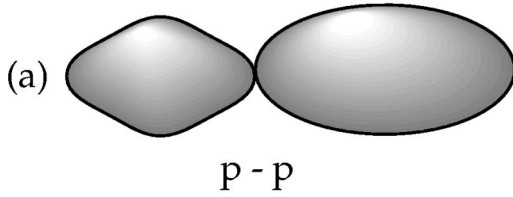


FIG. 2. (a) Pole-pole, (b) equator-equator, and (c) equator-equator twisted orientations for two touching deformed nuclei. The projectile has positive quadrupole and hexadecupole deformations, whereas the target is only prolate deformed.

$$\begin{aligned} \tilde{V}(\mathbf{q}) = & \sum_{\lambda_1 \mu_1} \sum_{\lambda_2 \mu_2} i^{\lambda_1 - \lambda_2} D_{\mu_1 0}^{\lambda_1}(\omega_1) D_{\mu_2 0}^{\lambda_2}(\omega_2) Y_{\lambda_1 \mu_1} \\ & \times (\Omega_q) Y_{\lambda_2 \mu_2}(\Omega_q) \tilde{\rho}_{\lambda_1}(q) \tilde{\rho}_{\lambda_2}(q) \tilde{v}(q). \end{aligned} \quad (14)$$

In the above formula we adopted the condensed notation ω_i for each set of Euler angles. Introducing Eqs. (14) and (10) into Eq. (3), the double-folding potential (1) is obtained in the multipolar form,

$$\begin{aligned} V(\mathbf{R}) = & \frac{1}{(2\pi)^3} \sum_{\lambda_i \mu_i} i^{\lambda_1 - \lambda_2 - \lambda_3} \hat{\lambda}_1 \hat{\lambda}_2 \hat{\lambda}_3^2 \begin{pmatrix} \lambda_1 & \lambda_2 & \lambda_3 \\ 0 & 0 & 0 \end{pmatrix} \\ & \times \begin{pmatrix} \lambda_1 & \lambda_2 & \lambda_3 \\ \mu_1 & \mu_2 & \mu_3 \end{pmatrix} D_{\mu_1 0}^{\lambda_1}(\omega_1) D_{\mu_2 0}^{\lambda_2}(\omega_2) D_{\mu_3 0}^{\lambda_3} \\ & \times (\Phi, \Theta, 0) F_{\lambda_1 \lambda_2 \lambda_3}(R), \end{aligned} \quad (15)$$

with the radial part given by the oscillating integral,

$$F_{\lambda_1 \lambda_2 \lambda_3}(R) = \int dq q^2 \tilde{\rho}_{\lambda_1}(q) \tilde{\rho}_{\lambda_2}(q) j_{\lambda_3}(qR) \tilde{v}(q). \quad (16)$$

Above, Φ and Θ are giving the orientation of the molecular system with respect to the laboratory system. Then Eq. (15) can be rewritten in a more condensed form in which the radial and angular parts are factorizing,

$$\begin{aligned} V(\mathbf{R}) = & \sum_{\lambda_i \mu_i} V_{\lambda_1 \lambda_2 \lambda_3}^{\mu_1 \mu_2 \mu_3}(R) D_{\mu_1 0}^{\lambda_1}(\omega_1) \\ & \times D_{\mu_2 0}^{\lambda_2}(\omega_2) D_{\mu_3 0}^{\lambda_3}(\Phi, \Theta, 0). \end{aligned} \quad (17)$$

The radial multipoles are

$$\begin{aligned} V_{\lambda_1 \lambda_2 \lambda_3}^{\mu_1 \mu_2 \mu_3}(R) = & \frac{1}{(2\pi)^3} i^{\lambda_1 - \lambda_2 - \lambda_3} \hat{\lambda}_1 \hat{\lambda}_2 \hat{\lambda}_3^2 \begin{pmatrix} \lambda_1 & \lambda_2 & \lambda_3 \\ 0 & 0 & 0 \end{pmatrix} \\ & \times \begin{pmatrix} \lambda_1 & \lambda_2 & \lambda_3 \\ \mu_1 & \mu_2 & \mu_3 \end{pmatrix} F_{\lambda_1 \lambda_2 \lambda_3}(R). \end{aligned} \quad (18)$$

If the fission (molecular) axis is fixed in the laboratory frame, then one can choose $\Theta = \Phi = 0$, and $D_{\mu_3 0}^{\lambda_3}(\Phi, \Theta, 0) = \delta_{\mu_3 0}$, which leads to

$$\begin{aligned} V(\mathbf{R}) = & \frac{1}{2} \sum_{\lambda_i \mu_i} V_{\lambda_1 \lambda_2 \lambda_3}^{\mu_1 \mu_2 0}(R) (1 + (-)^{\lambda_1 + \lambda_2 - \lambda_3}) \\ & \times \cos \mu(\alpha_2 - \alpha_1) d_{\mu 0}^{\lambda_1}(\beta_1) d_{-\mu 0}^{\lambda_2}(\beta_2) \\ & + \frac{1}{2} \sum_{\lambda_i \mu_i} V_{\lambda_1 \lambda_2 \lambda_3}^{\mu_1 \mu_2 0}(R) (1 - (-)^{\lambda_1 + \lambda_2 - \lambda_3}) \\ & \times \sin \mu(\alpha_2 - \alpha_1) d_{\mu 0}^{\lambda_1}(\beta_1) d_{-\mu 0}^{\lambda_2}(\beta_2). \end{aligned} \quad (19)$$

Due to the $3j$ coefficient occurring in Eq. (18) with all the angular momentum projections equal to zero, the angular momenta must fulfill $\lambda_1 + \lambda_2 - \lambda_3 = \text{even}$, otherwise the $3j$

equals zero. Thence, the last line in the Eq. (19) cancels and the final expression of the double-folding potential reads

$$V(\mathbf{R}) = \sum_{\lambda_i \mu_i} V_{\lambda_1 \lambda_2 \lambda_3}^{\mu_1 \mu_2 0}(R) \cos \mu(\alpha_2 - \alpha_1) d_{\mu 0}^{\lambda_1}(\beta_1) d_{-\mu 0}^{\lambda_2}(\beta_2). \quad (20)$$

For v , we introduced the M3Y effective interaction in the form used in Ref. [9]. We introduced additionally a phenomenological repulsive core in the nuclear potential originating from the compression effects of the overlapping density following a suggestion from Ref. [7]. The compression has the role to modify the potential in the internal part, the M3Y barriers remaining unchanged. Details on the strength of the compression term can be found in Ref. [13].

III. VARIOUS COLD FISSION AND FUSION CONFIGURATIONS

In fission, the fragments are strongly polarized due to the nuclear forces, and accordingly their symmetry axes are aligned. Only fluctuations around this axial symmetry configuration are allowed [14]. This is justified experimentally by the small forward anisotropy of the angular distribution of prompt γ rays. Consequently, $\alpha_1 = \alpha_2 = 0$, and Eq. (20) becomes

$$V(\mathbf{R}) = \sum_{\lambda_i \mu_i} V_{\lambda_1 \lambda_2 \lambda_3}^{\mu_1 \mu_2 0}(R) d_{\mu 0}^{\lambda_1}(\beta_1) d_{-\mu 0}^{\lambda_2}(\beta_2). \quad (21)$$

The one-dimensional tunneling probability will be maximized for $\beta_1 = \beta_2 = 0$, and thus Eq. (21) reads

$$V(\mathbf{R}) = \sum_{\lambda_i} V_{\lambda_1 \lambda_2 \lambda_3}^{0 0 0}(R). \quad (22)$$

This configuration is known in the literature under the name *pole-to-pole* ($p-p$) [15] or *nose-to-nose*.

As discussed in Ref. [5], there are several configurations that are important in fusion reactions. The $p-p$ one was already discussed in the context of the binary cold fission reactions (see Ref. [13] for a review).

In the *equator-equator* ($e-e$) or *belly-to-belly* orientation, the axial symmetric fragments are in touch with their symmetry axis parallel to each other. Then $\alpha_1 = \alpha_2 = 0$ and $\beta_1 = \beta_2 = \pi/2$.

Other configurations, relevant for fusion, according to [5] are the *pole-equator* ($p-e$) or the *nose-to-belly* orientation when $\alpha_1 = \alpha_2 = 0$, $\beta_1 = 0$, $\beta_2 = \pi/2$ and the *equator-equator twisted* ($e-c$) or the *crossed bellies* when $\alpha_1 = 0$, $\alpha_2 = \pi/2$, $\beta_1 = \beta_2 = \pi/2$. Some of these configurations are displayed in Fig. 2.

To illustrate in a very simple way the influence of the orientation in fusion, we consider the projectile-target system $^{238}\text{U} + ^{48}\text{Ca}$ used in the synthesis of the superheavy nucleus $^{286}112$ [16], with the symmetry axes found in the same plane. In this case the only degree of freedom describing the relative orientation is given by the angle $\beta_2 \equiv \theta$ between the molecular axis and the symmetry axis of the target. As one

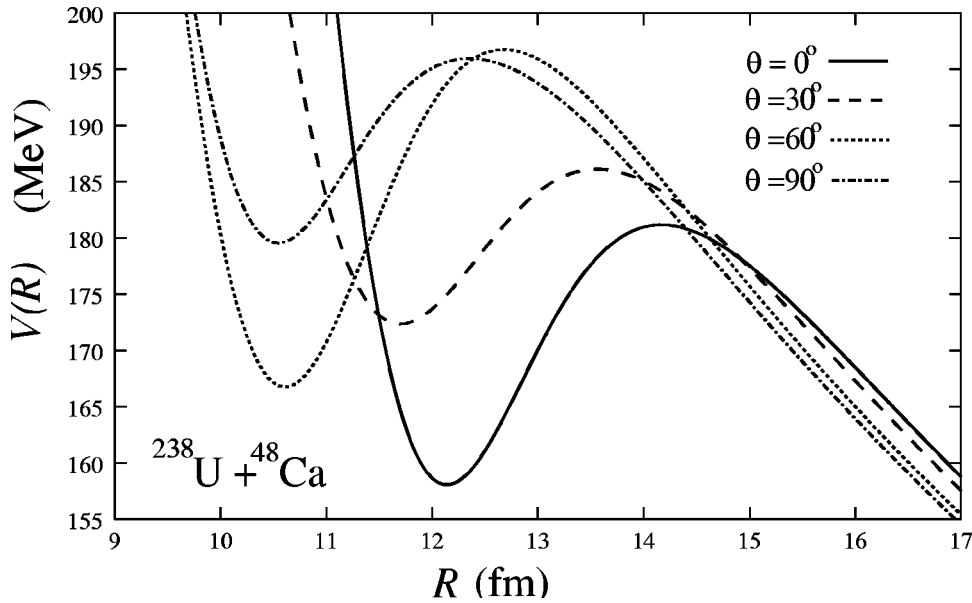


FIG. 3. The heavy-ion potential for the $^{238}\text{U}+^{48}\text{Ca}$ system in four different orientations of the projectile, i.e., $\theta=0^\circ$ (*pole-pole*), 30° , 60° , and 90° (*equator-equator*).

can see in Fig. 3 for each orientation of the ^{238}U target, pockets in the heavy-ion potential are possible. The difference is that the barrier is increasing with θ up to approximately 60° , afterwards the barrier decreases slightly. In Fig. 4, we show the density contour plots for the four above mentioned orientations. Contrary to the pure cold fission case where only one energy corresponds to a given fragmentation,

namely, the decay energy (and the configuration was shown to be of the type $p-p$), in the cold fusion, when the projectile and target are colliding at different orientations, a certain range of values of the bombarding energy should be considered. For bombarding energies that are noticeably higher than the height of the $p-p$ barrier, the fragments can scatter without undergoing mutual capture. When collision takes

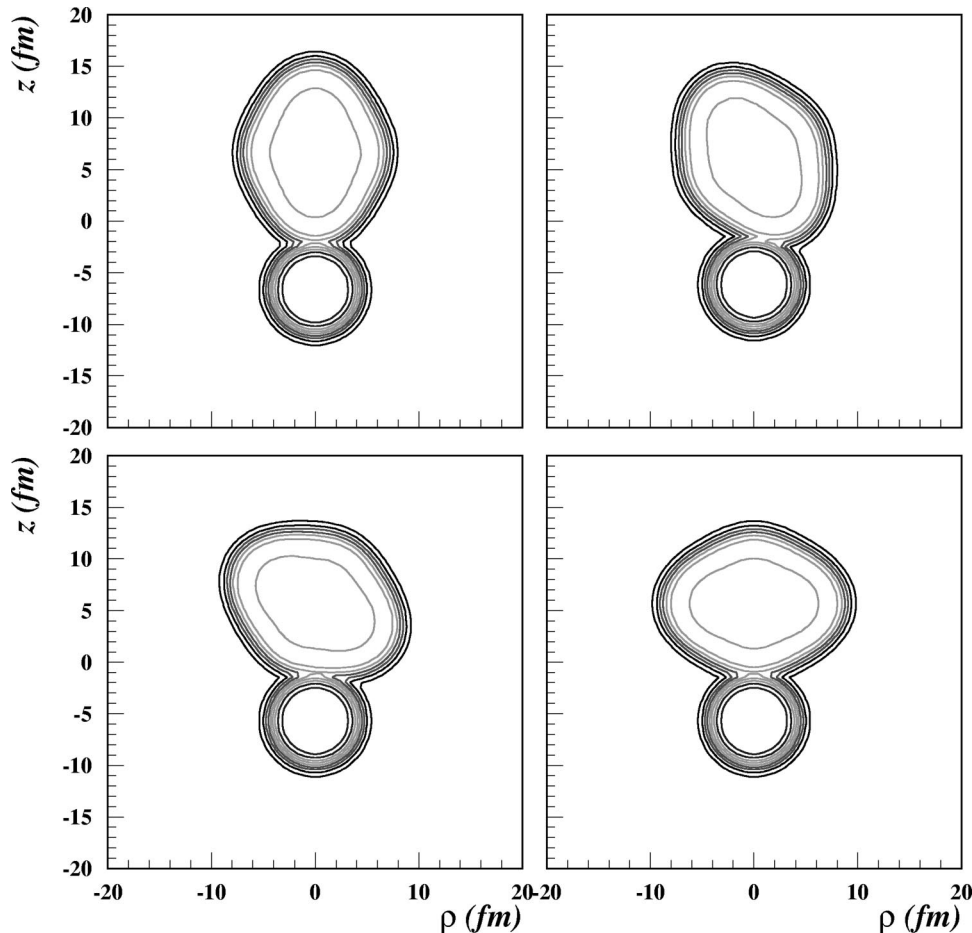


FIG. 4. Density contours for the $^{238}\text{U}+^{48}\text{Ca}$ system in the touching configuration using the deformations calculated in Ref. [11] for the same orientations as in Fig. 3.

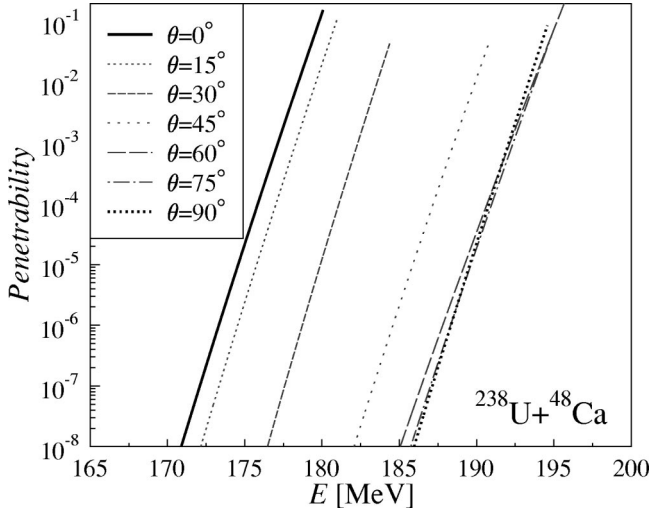


FIG. 5. Dependence of the one-dimensional barrier penetrability on the bombarding energy for the $^{238}\text{U}+^{48}\text{Ca}$ system for different orientations.

place for nonaxial-symmetric configurations, the capture probability for higher energy will take over the lower energy. This can be seen by plotting the one-dimensional penetrability as a function of the bombarding energy for different orientation angles (see Fig. 5),

$$P(E; \theta) = \exp\left(-\frac{2}{\hbar} \int_{r_1(\theta)}^{r_2(\theta)} \sqrt{2\mu(V(R, \theta) - E)} dR\right), \quad (23)$$

where $r_1(\theta)$ and $r_2(\theta)$ are the turning points.

The essence of Fig. 3 is that a certain energy can lead to a hot fusion process for a p - p orientation, but for another one, say e - e , it can rather lead to a cold fusion process.

IV. ORIENTATION DEPENDENCE OF THE DRIVING POTENTIAL

In the middle of seventies, it was suggested by Săndulescu and co-workers [17,18] to use projectiles such as ^{48}Ca , ^{54}Cr , ^{64}Ni , ^{70}Zn , and ^{76}Ge for the synthesis of super-heavy elements with $Z \leq 108$ in the compound nucleus reactions with ^{208}Pb . The basic idea of this approach was to calculate the potential energy surface of a given compound nucleus for all possible projectile-target combinations as a function of the mass and charge asymmetries, $\eta = (A_1 - A_2)/(A_1 + A_2)$ and $\eta_Z = (Z_1 - Z_2)/(Z_1 + Z_2)$ at the touching point R_c , i.e., the point where the assumed spherical fragments are coming in contact, and they interact only by means of the Coulomb force. The charges of the target and the projectile were determined by requiring that for a fixed η , the potential $V(R, \eta, \eta_Z)$ attains a minimum in the η_z direction, i.e., for every fixed mass pair (A_1, A_2) a single pair of charges is determined among all possible combinations.

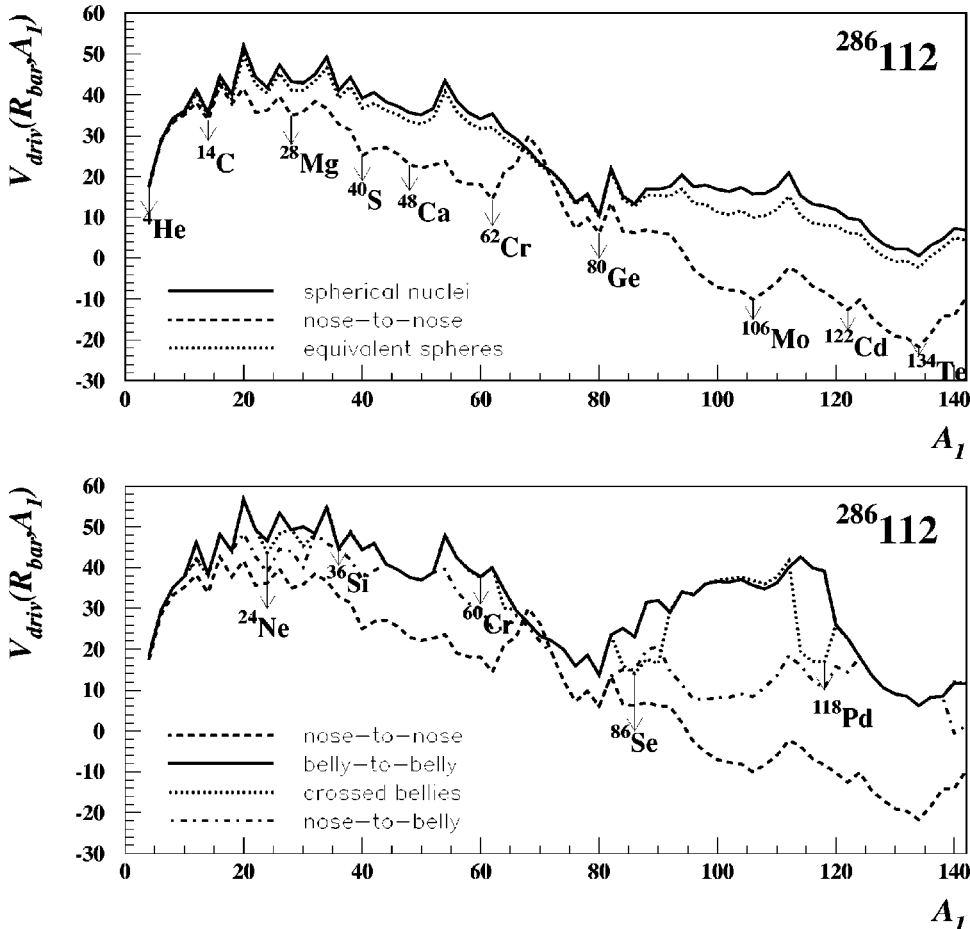


FIG. 6. Driving potential as a function of the projectile mass A_1 for the element $^{286}112$. On the upper panel, the driving potential along the A_1 coordinate at $R = R_{\text{bar}}$ is represented for spherical fragments (full line), for deformed fragments oriented in nose-to-nose configuration (dashed lines), and for the averaged orientation (dotted lines). On the lower panel the four curves correspond to the orientations nose-to-nose (dashed line), belly-to-belly (full line), crossed bellies (dotted lines), and nose-to-belly (dot-dashed).

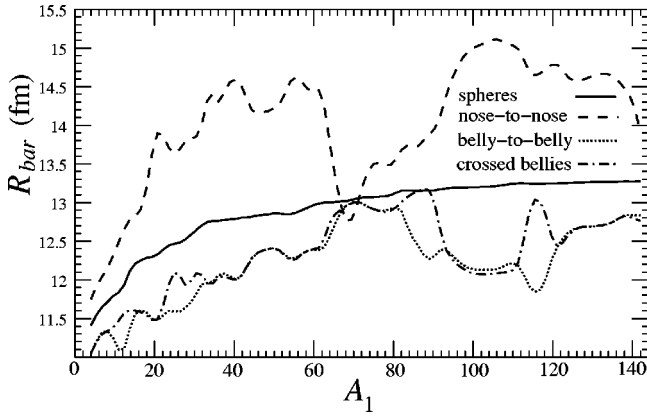


FIG. 7. The position of the barrier R_{bar} as a function of the light cluster mass for spherical nuclei (full curve), nose-to-nose (dashed lines), belly-to-belly (dotted lines), and crossed bellies (dot-dashed lines).

Next, minimas of the potential on the two-dimensional (R, η) landscape were searched. From here a criterion was inferred for cold fusion, i.e., the deep minima of the two-dimensional function $V(R, \eta)$ corresponds to the projectile-target combinations where the compound nucleus has a minimum of excitation and deexcite to the ground state with the emission of a couple of neutrons [19].

It is a well understood fact that the mass-asymmetry valleys that appear in the fragmentation potential are due to the shell effects. They are responsible for the maximum of cross sections for the same compound system obtained by different projectile-target combinations. It was advocated in Ref. [20],

using the framework of fragmentation theory, that due to the existence of different mass-asymmetry valleys for the same compound system, a new, highly asymmetric fission mode appears in which one of the fragments is close to the double magic nucleus ^{208}Pb . In all these calculations from the middle of seventies, the projectile and the target are considered to be spherical, and therefore the orientation plays no role.

In more recent calculations [21], taking again spherical projectiles and targets, the nuclear deformation energy of the elements $^{280}\text{108}$, $^{298}\text{114}$, and $^{304}\text{120}$ was studied using the macroscopic-microscopic method. Two mass valleys were found: a nearly symmetric one in which the projectile is very close to the double-magic ^{132}Sn , and a second one, very asymmetric related to the double-magic ^{208}Pb .

It is worthwhile to notice that these types of calculations, using the above mentioned spherical fragments, are producing valleys that are not too deep.

In what follows, we consider only the s channel in the fusion reactions, i.e., the orbital angular momentum is 0, and projectile and target are allowed to approach each other with various orientations specified by the Euler angles $\omega_i = (\theta_i, \phi_i)$, $i = 1, 2$. In order to avoid confusion between the second Euler angle and the deformation, we introduced a new notation for the angles (α, β) , that is (ϕ, θ) . Then, the driving potential is defined as [22]

$$V_{\text{driv}} = V(R, Z_1, A_1, \{\beta^{(1)}\}_{2,3,4}, \{\beta^{(2)}\}_{2,3,4}, \omega_1, \omega_2) + B_1 + B_2 - B_{\text{CN}}. \quad (24)$$

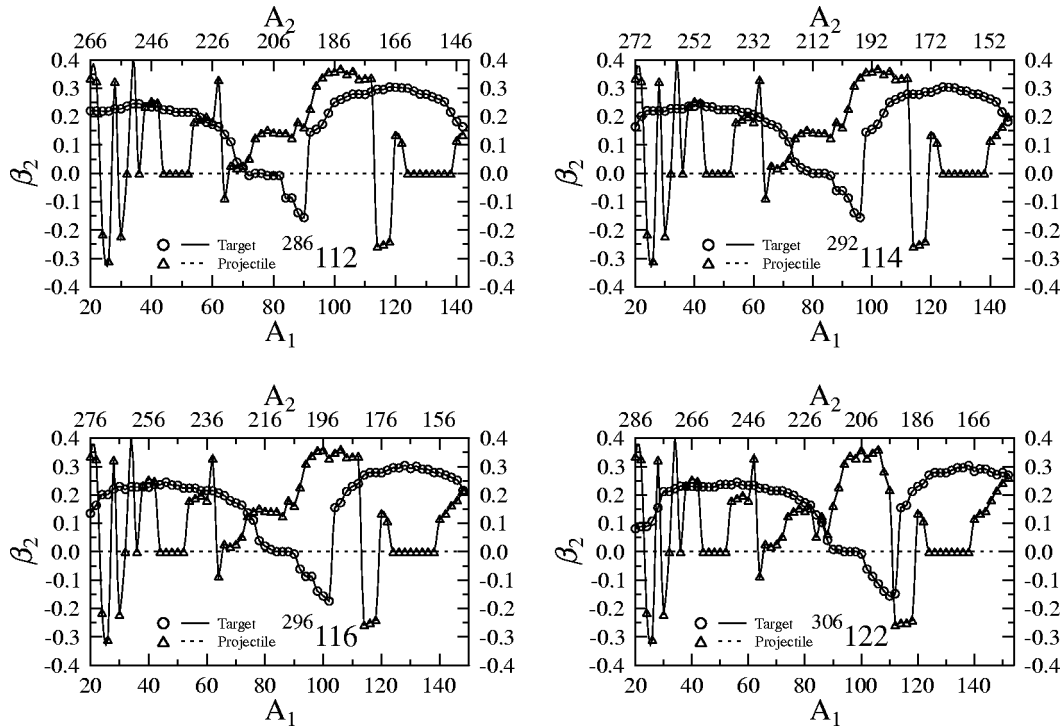


FIG. 8. Quadrupole deformations of the projectile A_1 (triangles) and target A_2 (circles) for the four superheavy nuclei studied in the present paper.

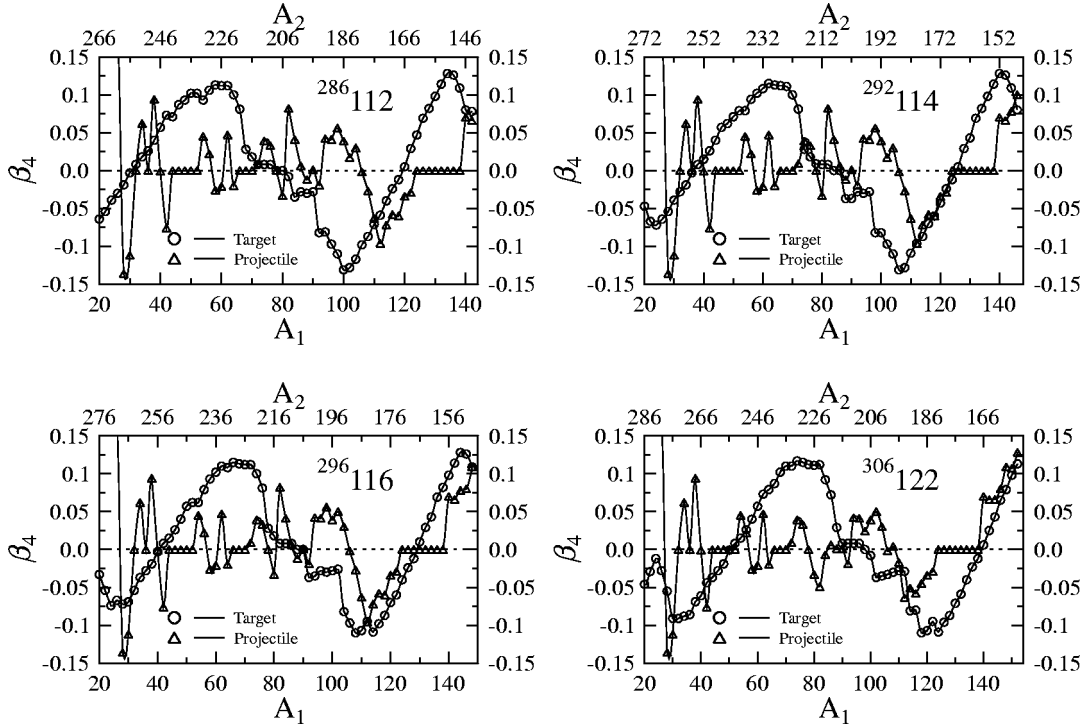


FIG. 9. Hexadecupole deformations of the projectile A_1 (triangles) and target A_2 (circles) for the four superheavy nuclei studied in the present paper.

Here B_1 , B_2 , and B_{CN} are the binding energies of the projectile, target, and compound superheavy nucleus. The driving potential also depends on the charges, masses, the distance between the centers of masses of the two nuclei, mutual orientations, and the quadrupole, octupole, and hexadecupole deformations through the heavy-ion potential V defined in Eq. (20).

In the study of formation of dinuclear molecules, when the target is deformed and the projectile spherical, the sub-barrier fusion cross section is computed by replacing the deformed nucleus with a series of spherical nuclei of different radii [23,24]. The potential is then averaged over the angles of orientation to get an effective potential. In the present case when both projectile and target can be deformed the averaging formula reads

$$\bar{V}_{\text{driv}} = \frac{\int V_{\text{driv}}(\omega_1, \omega_2) d\omega_1 d\omega_2}{\int d\omega_1 d\omega_2}. \quad (25)$$

A simple evaluation of the above integral, using the multipolar decomposition of the double-folding potential (20) leads us to the result that the orientation-averaged driving potential \bar{V}_{driv} coincides with the monopolar component of the driving potential. For this reason, we expect similarities between the orientation-averaged driving potential of two deformed nuclei and the driving potential in the approximation of spherical nuclei.

We follow the same procedure as in Ref. [17], and search first for minima of the driving potential in the landscape

(Z_1, Z_2) for a fixed mass pair (A_1, A_2). As a result, we obtain for each orientation (ω_1, ω_2) the driving potential as a function of the center-to-center distance R and the mass number of the projectile (target).

As a case study, we compute the cold fusion driving potentials of the superheavy nuclei $^{286}_{112}$, $^{292}_{114}$, $^{296}_{116}$, and $^{306}_{122}$ which were recently investigated by the group from FLNR Dubna [25]. The target nuclei ^{238}U , ^{244}Pu , and ^{248}Cm were bombarded with ^{48}Ca projectiles, and it was observed that the mass distribution of fission fragments of compound nuclei is asymmetric in shape with the light fragment mass having an average of 132–134. For the element 122, the projectile ^{56}Fe was used to bombard ^{248}Cm .

A. The nucleus $^{286}_{112}$

In Fig. 6 we represented a cut along the mass-asymmetry coordinate of the driving potential. The center-to-center distance of the fragments was fixed at the value of the barrier R_{bar} whose geometrical locus is plotted in Fig. 7 for four orientations. As it is easy to notice that the position of the barrier is varying very smoothly when the projectile and the target are taken to be spherical. For nose-to-nose oriented fragments the transition from regions of prolate deformations to regions of oblate deformations determines large fluctuations in the geometrical locus of R_{bar} . These oscillations are less pronounced for $e-e$ and $e-c$ orientations.

From the inspection of Fig. 6, we remark the differences in the driving potential when the target and the projectile are spherical and when they are deformed. In all the calculations we included quadrupole, octupole, and hexadecupole deformations. The Ca valley (with heavy partner U) is more pro-

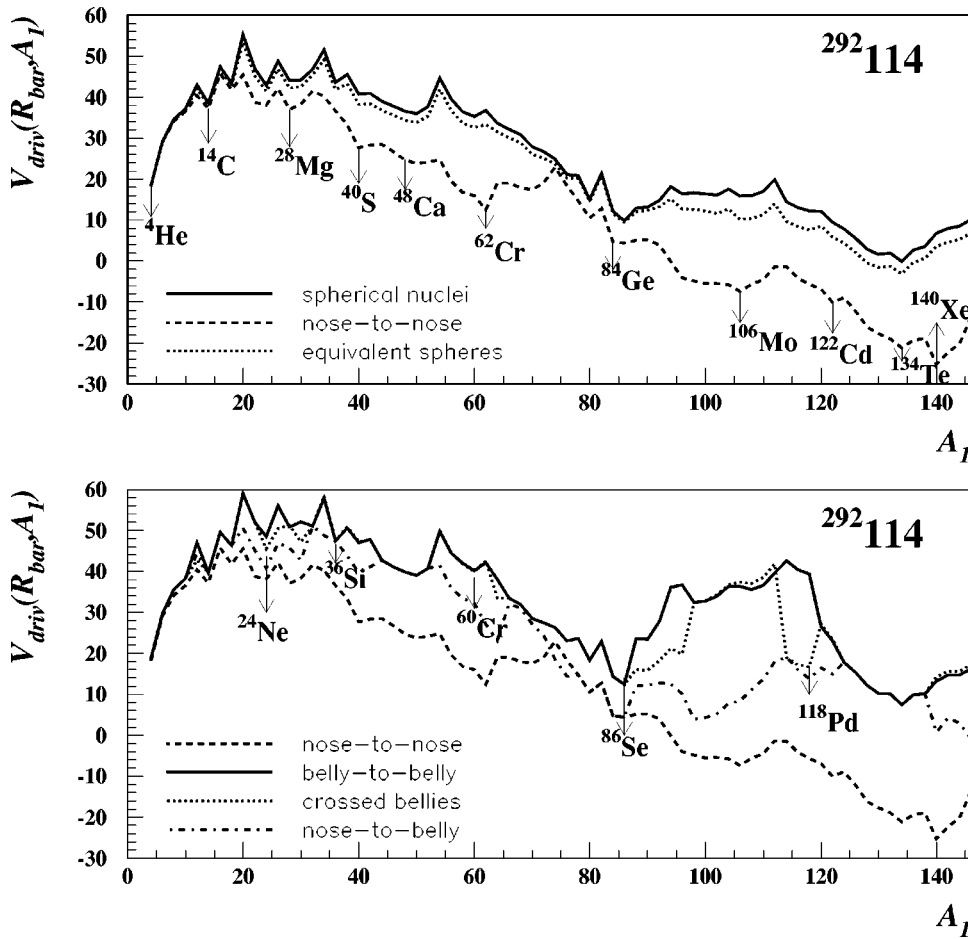


FIG. 10. Same as in Fig. 6, but for the nucleus $^{292}_{114}$.

nounced when one takes spherical fragments or when the fragments are coming in contact in $e-e$ or $e-c$ orientations. The valleys corresponding to the cluster radioactivity (superasymmetric valleys) are occurring with some differences: for $p-p$, the most pronounced are ^{14}C , ^{22}Ne , and ^{28}Mg , whereas for $e-c$ we remark ^{24}Ne , ^{30}Mg , and ^{36}Si .

For $p-p$ oriented fragments, the valley centered on ^{62}Cr is separated by a high barrier from what we call the Pb valley centered on ^{76}Zn and ^{80}Ge , and obviously for such configurations the tendency of the initial cold strong asymmetric system to move in the symmetric direction, before undergoing quasifission, is hindered.

The $p-e$ orientation presents features common to the $p-p$ but also to the $e-e$ and $e-c$ orientations. Similar to the $p-p$ case, the valley for Ca is less pronounced and the Mo valley is broader and the target ^{96}Sr will give a minimum in the potential for this orientation.

For the $e-c$ orientation we notice a valley, coming after the Pb valley, centered on ^{86}Se , which also contains ^{90}Kr . For this orientation there is an additional valley centered on ^{118}Pd , which is connected to the prolate-to-oblate transition in this mass region of the target, as can be observed on the top-left panel of Fig. 8 and the region of negative hexadecupole deformations (slightly necked shapes) of both projectile and target (see the top-left panel of Fig. 9). This valley occurs also for the elements 114 and 116, due to the same reasons. For $e-e$ orientations these two valleys are disappear-

ing. Between the Pb valley and the valley centered on ^{134}Te , which contains also Sn, a huge barrier is showing up, which determines an even stronger hindrance to symmetric quasifission compared to $p-p$ orientation.

The orientation-averaged potential follows very closely the spherical one, the differences in the barrier height being more sensitive in the weak asymmetric and symmetric regions. This characteristic is the same for all superheavy nuclei studied in this paper.

B. The nucleus $^{292}_{114}$

For the driving potential of the superheavy nucleus $^{292}_{114}$ (see Fig. 10), we remark a similar structure of $p-p$ and $e-e$ valleys as for $^{286}_{112}$: a nearly symmetric valley with the minimum displaced at ^{140}Xe for the $p-p$ configuration, a broad asymmetric valley centered on ^{106}Mo (which contains also Zr isotopes and arises only for $p-p$ orientations), the deep Cr valley (in combination with U), a very asymmetric shallow valley centered on $^{84}\text{Ge}+^{208}\text{Pb}$ for the $p-p$ orientation, and a deep valley centered on ^{86}Se for the $e-e$ and $e-c$ orientations. In other calculations this valley is assigned to Kr [26]. One should note that the occurrence of this deep valley is motivated by the transition to oblate deformations of the target as can be observed on the top-right panel of Fig. 8. In the present study a few of Kr isotopes are occurring in the $e-e$ and $e-c$ valleys. The valley corresponding to ^{48}Ca (in

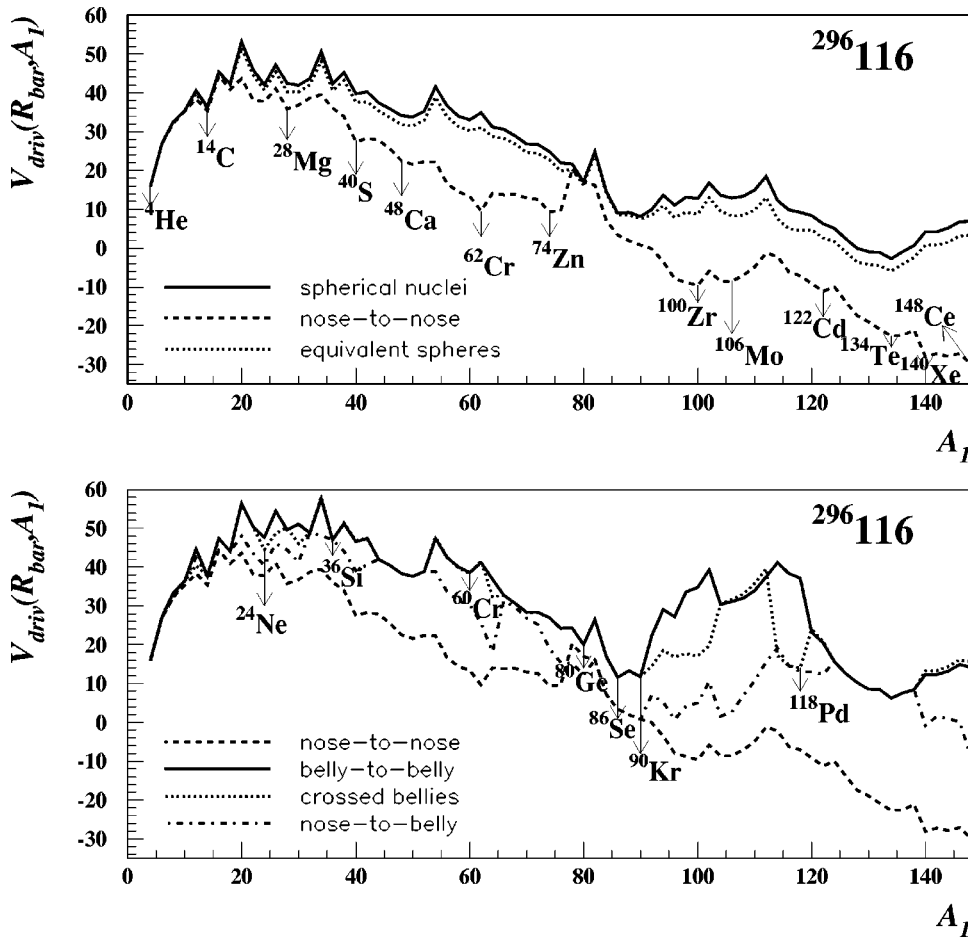


FIG. 11. Same as in Fig. 6, but for the nucleus $^{296}_{116}$.

combination with ^{248}Cm) is less pronounced for the p - p orientations, but when the fragments are constrained to be spherical or to collide in the belly-to-belly or crossed-bellies orientation, this valley becomes more pronounced.

As for the p - e orientation we remark the increase in importance of the ^{98}Sr nucleus simultaneously with the vanishing of the Mo minimum. The Cr valley, which occurred for the p - p orientation is now shifted to ^{64}Fe such that we deal with the Fe valley frequently invoked in the literature [27].

C. The nucleus $^{296}_{116}$

For the nucleus $^{296}_{116}$ the new features are the entrance in competition with the Cr-Fe valley of a neighboring valley centered on ^{74}Zn for the p - p orientation, the entrance of ^{90}Kr in competition with ^{86}Se for the Pb valley in e - e and e - c orientations and the occurrence of a second minimum (^{100}Zr) in the Mo valley for the p - p orientations (Fig. 11). Like in the previous case the accentuation of the Pb valley for the e - e and e - c orientations is a consequence of the prolate-to-oblate transition of the target (bottom-left panel of Fig. 8) and small negative hexadecupole deformations of both nuclei.

Contrary to the nuclei $^{286}_{112}$ and $^{292}_{114}$, for $^{296}_{116}$ an absolute minimum occurs for fully symmetric fragmentation, i.e., $^{148}\text{Ce} + ^{148}\text{Ce}$ in p - p configuration.

In the case of the p - e orientation the Fe valley is gaining more stability.

D. The nucleus $^{306}_{122}$

We next go six units higher in charge, to the superheavy nucleus $^{306}_{122}$, in order to investigate possible deviations from the above observed pattern of cold fusion valleys formation.

For the p - p orientation we notice two main valleys, one corresponding to Mo-Zr, already observed for the previous superheavy nuclei and another one to Ge. This last valley gains in importance in comparison to the previously superheavy nuclei due to the occurrence of large deformations of the Th target. In this case the Pb valley is melting with the Mo-Zr valley since Pb comes in combination with Zr. For the orientations p - e and e - e , it is only the Pb part of this valley which survives, whereas for e - c it vanishes (Fig. 12).

The tendency observed to $^{296}_{116}$ to form a valley for total symmetry ($\eta=0$) and p - p orientation will be now even more accentuated, which could lead to a high quasifission yield for symmetric separation if the p - p scenario would work for cold fusion.

For e - c orientation we obtain a new valley centered on ^{112}Ru . In this region both projectile and targets have negative hexadecupole deformations, as can be noticed from the bottom-right panel of Fig. 8.

For the p - e orientation we remark the constancy of the valley centered on ^{64}Fe and the fact that the leading role in the Mo-Zr valley, specific for the p - p orientation, is now taken over by ^{100}Zr that comes in combination with the

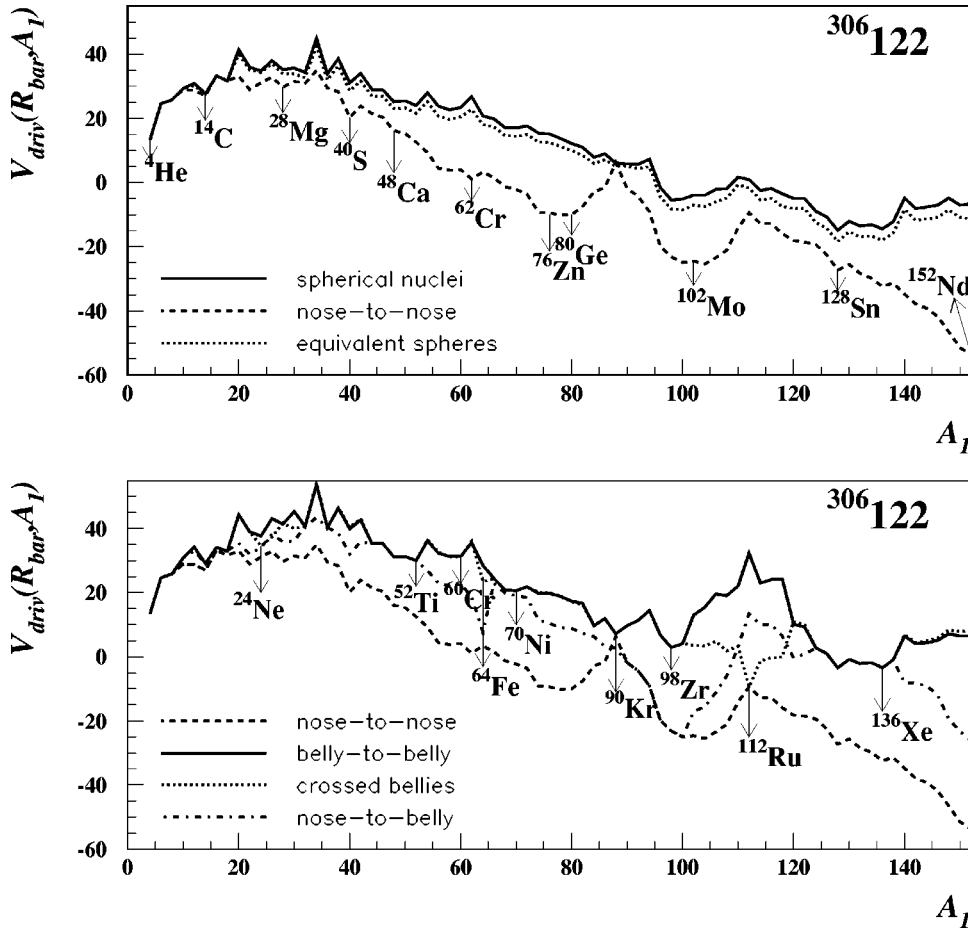


FIG. 12. Same as in Fig. 6, but for the nucleus $^{306}_{122}$.

double-magic ^{208}Pb . This valley is separated from the total symmetric valley by a broad barrier, contrary to the $p-p$ case.

In the cluster radioactivity region we notice the occurrence of a narrow valley for ^{32}Si .

V. CONCLUSIONS

In this paper we tried to understand the role of mutual orientation of the fragments in the formation of cold fusion valleys. Especially due to the existence of quadrupole and hexadecupole deformations the various orientations will produce different valley structures in the fusion potential.

According to earlier calculations in which the fragments are taken to have at most positive quadrupole deformations and the barrier is constructed by using the nuclear proximity potential [27], for the elements 112, 114, and 116, two valleys are substantiated, one corresponding to Fe and the other one to Pb. The deformations used in the present study are provided by recent improved calculations of the macroscopic-microscopic model [11] which take into account also octupole and hexadecupole distortions of the nuclear shape and an exhaustive systematics of the nuclear binding energy for several thousands of nuclei ranging from ^{16}O to the superheavy nucleus $^{339}_{136}$. Consequently, we obtain a richer structure of valleys.

The main reason for the importance of the Mo valley, for all superheavy nuclei studied in this paper, in the $p-p$ orientation is the existence of noticeable prolate deformations for

both projectile and target. In what concerns the Ge valley, the things are different. Only the target does not have too large deformation for the nucleus $^{286}_{112}$, and the reason why ^{80}Ge dominates a very shallow valley can be explained by the sensitive decrease of the Q value for the reaction $^{80}\text{Ge} + ^{206}\text{Hg} \rightarrow ^{286}_{112}$. For the synthesis of $^{306}_{122}$, the isotope Ge enters in combination with well deformed prolate isotopes of Th, and therefore the corresponding valley will gain in importance. However, it should be noted that for spherical projectile-target pairs or for $e-e$ and $e-c$ orientations, the Ge valley is disappearing.

We remarked also the occurrence of Sn isotopes in a weak asymmetric valley, but not of the double-magic ^{132}Sn . As for the double-magic nucleus ^{208}Pb we arrived at the conclusion that the corresponding valleys in the driving potential are especially pronounced for the $e-e$ and $e-c$ orientations, and to a lesser extent for $p-e$. In contrast to these orientations, the $p-p$ driving potential exhibits a very shallow Pb valley.

We showed also that the orientation-averaged driving potential resembles very much the driving potential with spherical projectile-target pairs.

It is obvious from the inspection of driving potential cuts along the mass-asymmetry coordinate that the $p-p$ orientation is unlikely to explain the experimental observation of asymmetric distribution of fission fragments. Deep cold valleys including the light fragments with masses 132–134 were found in the present study for all studied configura-

tions, including the orientation-averaged case, except the p - p case. This can be understood, according to our opinion, whether by the realization of the orientation-averaged scenario for quasifission fragments, and not for the fission fragments, or by the fission of the compound nucleus along channels other than the p - p one. This last scenario, contrasting to the scenario widely accepted for the cold fission of ^{252}Cf , when the fragments are emerging in p - p configuration, may be for the moment justified only qualitatively by the possibility to populate the states from the oblate well due to the available excitation energy in the compound nucleus. The decisive answer to this challenging problem requests naturally more experimental information.

Although some of the predicted fusion valleys are not found in previous works, we should notice that several of the neutron-rich isotopes creating these valleys (^{100}Zr , ^{106}Mo , ^{112}Ru , ^{148}Ce , ^{140}Xe) were recently recorded in the cold binary fission of ^{252}Cf [28]. In the cluster radioactivity region we observe the valleys for ^{14}C , ^{24}Ne , and ^{28}Mg , clusters that were earlier observed to be emitted from the parent nuclei ^{224}Ra , ^{234}U , ^{238}Pu (see Ref. [29], and references therein).

As noted in Ref. [5], it was Nörenberg who suggested first the use of two well-deformed rare-earth nuclei in an equator-equator twisted orientation in fusion, for the simplest reason that such an orientation leads to the most compact touching

configuration out of all possible orientations of two deformed nuclei. In this paper we showed quantitatively the occurrence of fusion cold valleys for such orientations in all cases. For the superheavy nuclei $^{286}112$, $^{292}114$, and $^{296}116$ this valley corresponds to ^{118}Pd ; whereas for $^{306}122$ the valley is centered on ^{112}Ru .

It should be noted that according to the relativistic mean field, the nucleus with proton number $Z=120$ and neutron number $N=172$ is predicted to be double magic. Nuclei near to this value of N and Z are expected to be also spherical and therefore the argument that collisions in the equator-equator twisted orientation are geometrically more suitable than the pole-to-pole one in the synthesis of a spherical superheavy nucleus seems to gain support.

ACKNOWLEDGMENTS

One of the authors (Ş.M.) would like to acknowledge the financial support from the European Community through a Marie Curie fellowship, Contract No. HPMF-CT-2000-00417. He is also grateful to Professor A. Sandulescu, Dr. F. Carstoiu, and Dr. A. Nasirov for enlightening discussions. Both authors express thanks to Dr. Th. Bürvenich for reading the manuscript. The technical assistance of Astrid Steidl in designing Figs. 1 and 2 is kindly acknowledged.

-
- [1] W. Greiner, J.Y. Park, and W. Scheid, *Nuclear Molecules* (World Scientific, Singapore, 1995).
- [2] R. Bass, *Nuclear Reactions with Heavy Ions* (Springer-Verlag, Berlin, 1980).
- [3] Ş. Mişicu, A. Săndulescu, and W. Greiner, *Phys. Rev. C* **64**, 044610 (2001).
- [4] A. Săndulescu, Ş. Mişicu, F. Cârstoiu, A. Florescu, and W. Greiner, *Phys. Rev. C* **57**, 2321 (1998).
- [5] A. Iwamoto, P. Möller, J. Rayford Nix, and H. Sagawa, *Nucl. Phys. A* **596**, 329 (1996).
- [6] R. Maas and W. Scheid, *J. Phys. G* **16**, 1359 (1990).
- [7] E. Uegaki and Y. Abe, *Prog. Theor. Phys.* **90**, 615 (1993).
- [8] J. Schmidt and W. Scheid, *Phys. Rev. C* **53**, 322 (1996).
- [9] A. Săndulescu, Ş. Mişicu, F. Cârstoiu, and W. Greiner, *Elem. Chastits At. Yadra* **30**, 908 (1999) [*Phys. Part. Nucl.* **30**, 386 (1999)].
- [10] G.R. Satchler, *Direct Nuclear Reactions* (Clarendon, Oxford, 1983).
- [11] P. Möller, J.R. Nix, W.D. Myers, and W.J. Swyatecki, *At. Data Nucl. Data Tables* **59**, 185 (1995).
- [12] D.A. Varshalovich, A.N. Moskalev, and V.K. Khersonskii, *Kvantovaya Teoriya Uglovogo Momenta* (Izdatelstvo Nauka, Leningrad, 1975) [English translation: *Quantum Theory of Angular Momentum* (World Scientific, Singapore, 1988)].
- [13] A. Săndulescu and Ş. Mişicu, in *Cluster Radioactivity, Fission, Fusion and the Superheavy Nuclei*, CCAST-WL Workshop Series Vol. 123 (CCAST-WL, Beijing, 2000), p. 31.
- [14] Ş. Mişicu, A. Săndulescu, G.M. Ter-Akopian, and W. Greiner, *Phys. Rev. C* **60**, 034613 (1999).
- [15] P.O. Hess and W. Greiner, Jr., *Nuovo Cimento Soc. Ital. Fis.*, A **83A**, 77 (1984).
- [16] Yu.Ts. Oganessian, *Nucl. Phys.* **A682**, 108c (2001).
- [17] A. Săndulescu, R.K. Gupta, W. Scheid, and W. Greiner, *Phys. Lett.* **60B**, 225 (1976).
- [18] R.K. Gupta, A. Săndulescu, and W. Greiner, *Phys. Lett.* **67B**, 257 (1976).
- [19] R.K. Gupta, C. Părvulescu, A. Săndulescu, and W. Greiner, *Z. Phys. A* **283**, 217 (1977).
- [20] A. Săndulescu and W. Greiner, *J. Phys. G* **3**, L189 (1977).
- [21] R.A. Gherghescu, D.N. Poenaru, and W. Greiner, *J. Phys. G* **23**, 1715 (1997).
- [22] G. Giardina, S. Hofmann, A.I. Muminov, and A.K. Nasirov, *Eur. J. Phys.* **8**, 205 (2000).
- [23] R.G. Stokstad and E.E. Gross, *Phys. Rev. C* **23**, 281 (1981).
- [24] T. Arctadius and Chr. Bargholz, *Z. Phys. A* **335**, 315 (1990).
- [25] M.G. Itkis *et al.*, in *Proceedings of the International Workshop on Fusion Dynamics at the Extremes*, edited by Yu. Ts. Oganessian and V.I. Zagrebaev (World Scientific, Singapore, 2001), p. 93.
- [26] R.K. Gupta, M. Balasubramanian, G. Münzenberg, W. Greiner, and W. Scheid, *J. Phys. G* **27**, 867 (2001).
- [27] A. Săndulescu and W. Greiner, *Rep. Prog. Phys.* **55**, 1423 (1992).
- [28] A.V. Ramayya *et al.*, in *Proceedings of the Second International Conference on Fission and Properties of Neutron Rich Nuclei*, edited by J.H. Hamilton, W.R. Philips, and H.K. Carter (World Scientific, Singapore, 1999), p. 246.
- [29] R.K. Gupta and W. Greiner, *Int. J. Mod. Phys. E* **3**, 335 (1994).